Ag_2CO_3 / magnetic reduced graphene oxide nanocomposite as advanced visible light photocatalytic hybrid materials for efficient degradation of azo dye

Mohamed A. Elsayed[1,*], Hesham R. Tantawy[1], Amr A. Nada[2], Mohamed E. Elmowafy[1]

[1]*Chemical Engineering Department, Military Technical College, Cairo, Egypt*
[2]*Department of Analysis and Evaluation, Egyptian Petroleum Research Institute, Cairo, Nasr city P.B. 11727, Egypt*

[*]Corresponding author: E-mail: m.aboelfotoh@mtc.edu.eg

Received: 29 July 2018, Revised: 10 September 2018 and Accepted: 26 October 2018

DOI: 10.5185/amlett.2019.2189
www.vbripress.com/aml

Abstract

Due to intrinsic properties of graphene-like high electrical conductivity and large surface area, these properties make it an attractive matrix for composites. In this work, reduced graphene oxide (RG)/Fe_3O_4 (M)/Ag_2CO_3 (S) hybrid nano-composite (MRGS) has been effectively produced by coprecipitation techniques. The prepared composites were investigated by powder X-ray diffraction (XRD), Fourier transforms infrared spectra (FT-IR), transmission electron microscopy (TEM), UV-vis diffuse reflectance spectra (UV-vis/DRS), Raman and vibrating sample magnetometer (VSM). The prepared MRGS nano-composite shows significant enhancement in the degradation rate of Tartrazine dye (TZ) compared to commercial photo-catalyst such as TiO_2. Meanwhile, the visible light absorption of the MRGS nano-composite is progressively refining with the increase of the percentage of Ag_2CO_3 on the surface of (RG). The obtained MRGS 75 photo-catalyst shows the best photo-catalytic activity for TZ under visible light irradiation. The close contact between Ag_2CO_3 and RG in the composite leads to accelerating the charge transfer on Ag_2CO_3 to RG and thus enhancing the photocatalytic activity. Additionally, the prepared composite displays superb separability and significant stability.

Keywords: Magnetic graphene, photo-degradation, magnetic graphene silver carbonate and tartrazine dye.

Introduction

The significant properties of graphene such as; high electrical conductivity, high surface area, thermal, mechanical and optical properties make it a distinguishable matrix for nanocomposites. Therefore, incorporation of graphene with suitable materials has been the focus of research in recent years for their multifunctional abilities [**1**].

Graphene has been decorated with a different inorganic materials such as metals (Au [**2**], Ag **[3]**, Pt [**4**], Cu [**5**]), metal oxides (ZnO [**6**], TiO_2 [**7**], SnO_2 [**8**], Fe_3O_4 [**9**], Fe_2O_3 [**10**], NiO, MnO_2 [**11**]), metal sulphides (CdS [**12**], ZnS [**13**], MoS_2 [**14**] etc.) Such composites have great potentials for many applications like electrochemical sensing, super-capacitors, solar cells, lithium ion batteries and photo-catalysis [**15, 16**]. Among graphene-based metal nano-composites, the noble metals like silver (Ag) [**17**], gold [**2**], platinum [**18**], are the most reported in the literature as the second component due to their optical and catalytic properties. Incorporation of the two-dimensional graphene nano-sheets with noble metals is expected to enhance the properties of noble metals and graphene. For instance, in 2009, the reports showed the aggregation of Ag or Au nanoparticles on the surface of graphene nano-sheets, which were supported on flat silicon (Si) flake or Si nano-wells [**19**]. Beside noble metals, there are other metals like tin (Sn) [**20**], copper (Cu) [**21**], cobalt (Co) [**22**], alloys [**23**] and bimetals [**24**] have been reported to incorporate with graphene layers.

Graphene has been combined with various metal compounds like (ZnO [**6**], TiO_2 [**7**], SnO_2 [**8**], Fe_3O_4 [**9**], Fe_2O_3 [**10**], NiO [**25**], MnO_2 [**11**], etc.). Metal sulfides like (CdS [**12**], ZnS [**26**], MoS_2 [**14**], etc.) metal hydroxides like (Co $(OH)_2$ [**27**], Ni$(OH)_2$ [**28**], etc.). In addition to metals and metal compounds, non-metalic materials have also been used as a second component in graphene-based nano-composites like (S [**29**], Si [**30**], SiO_2 [**31**], etc.). Graphene has also been combined with other carbon materials like carbon black [**32**], carbon nanotube [**33**], carbon sphere [**34**], carbon nano-fibers [**35**] and fullerene [**36**], to produce new carbon materials.

Photolysis is a process of molecule dissociation via light energy. Photo-catalysis achieves the same

dissociative effects, but does so in the presence of a catalyst, consequently lowering the activation energy. Thus, photo-catalysis is a photochemical process whereby molecular dissociation takes place on a solid catalytic surface, typically a semiconducting metal oxide. Because photo-catalysis relies on photo-excitation, the prospect of utilizing ever abundant free solar energy received via sunlight remains considerably appealing [**37**].

The disadvantage of most of the semiconductor photo-catalysts like titanium dioxide (TiO_2) and silver carbonate (Ag_2CO_3) is the fast electron-hole recombination within photo-catalysts, which decreases the efficiency of its photo-catalytic activity. TiO_2 is well-known as one of the best photo-catalyst materials, and many reports have concentrated on the preparation and photo-catalytic applications of graphene-TiO_2 nano-composite

Silver materials and its derivative, such as Ag_2O [**38**], Ag_3VO_4 [**39**], Ag_3PO_4 [**40**], Ag_2CO_3 [**41**], AgX (X=I, Br, and Cl) [**42**]…….. etc. have been studied as efficient photo-catalysts for degradation of organic pollutants by many researchers. Previous papers realized that these silver derivatives demonstrate hopeful photo-catalytic effects; in addition, they are easy to work under the visible light because of its characteristics, photosensitivity and narrow band gap. Lately, between diverse silver materials, Ag_2CO_3 has been the most significant visible light driven catalyst. However, It is unstable materials, it demonstrates photo-corrosion which may be attributed to the Ag+, which may alter into metallic Ag via gain the photo-induced electrons in the photo-catalytic procedures and the excessive Ag may act as the recombination center of electrons and holes, resulting in the decrease of the photocatalytic activity [**43, 44**]. Many approaches were adapted to alter Ag_2CO_3 and expand the stability and photo-catalytic effect, such as overloaded onto C_3N_4 [**45**], BN [**46**], RG [**43**], etc.

In this work, graphene oxide (GO) was synthesized according to the hummer method. A suitable chemical reducing agent was employed to obtain the reduced form of GO (RGO). Different doping candidates (magnetite and silver carbonate) were selected to be loaded on the surface of RGO with different ratios. The visible light photo-catalytic potential of the obtained samples has been investigated on tartrazine as a reprehensive for the organic contaminant. The main target of this study is to prepare a composite with enhancement behavior capable of removing of organic contaminant efficiently from synthetic wastewater beneath visible light irradiation without any secondary contamination.

Experimental procedure and materials

Materials for preparation

Commercial graphite 99%, ammonia solution 35%, isopropyl alcohol 99.5%, Ferric chloride 99%, Sodium nitrate 99%, Potassium permanganate 98%, Sulfuric acid 98%, Hydrogen peroxide 35%, Ferrous Sulfate 99%, and tartrazine were purchased from Sigma Aldrich. The purities of all used materials were specified by a weight ratio.

Synthesis of the MRGS nano-composite

The utilized modified approach could be summarized as follows; graphite as a raw material (5 g) was oxidized to graphite oxide by mixing it with sodium nitrate (5 g) in sulfuric acid (250 ml). Potassium permanganate (30 g) is added to the mixture in portions, in an ice bath to do not allow the temperature to increase more than 5 ^oC to avoid the explosion. After adding all potassium permanganate, the mixture kept at room temperature for 1hr. Then the mixture is heated to 12 hours at 35 ^oC. Distilled water (1000 ml) is added to the mixture for hydrolysis and mixture is heated at 98 ^oC for 1 hour. Finally, hydrogen peroxide (50ml) is added at which the clear-yellowed color of graphene oxide is formed. The obtained final product is washed with distilled water to remove any remnant acid and dissolved salts. After that, GO was isolated by vacuum filtration from the solution and dried in an oven at 40 ^oC for 24 h. MRG was prepared by the co-precipitation method. Firstly, Fe_2SO_4 and $FeCl_3$ solutions were mixed by 1:2 molar ratio, respectively. Various amount of GO was sonicated for 20 min and then added to the previous mixtures to prepare different MRG compositions (MRG10, 20 and 30). Adjusting the pH to 10 by ammonia solution as mixtures were kept at 70 ^oC. The product was then separated and dried.

In order to prepare of Ag_2CO_3/MRG composite (MRGS), the optimum MRG has suspended in 50 ml solution of sodium carbonate in deionized water by ultrasonic treatment for 10 min. A solution of silver nitrate in 50ml deionized water was added by burette to the MRG suspension under mechanical stirring for 1 hr. Finally, the sample was separated by vacuum filtration from the solution and it was put in the oven at 60 ^oC. The (25, 50 and 75 %) MRGS catalyst was prepared with a ratio (3:1, 1:1 and 1:3 w/w) respectively of MRG and Ag_2CO_3 nanoparticles. Finally, the product was separated by filtration and dried in the oven at 70 ^oC. **Table 1** shows the sample name, abbreviations, and composition. The prepared composites were investigated by powder X-ray diffraction (XRD), Fourier transforms infrared spectra (FT-IR), transmission electron microscopy (TEM), UV-vis diffuse reflectance spectra (UV-vis/DRS), Raman and vibrating sample magnetometer (VSM).

Table 1. The sample name, abbreviations and composition.

Sample composition	Abbreviations
Graphene oxide	GO
Reduced graphene oxide	RGO
Magnetite/ reduced graphene oxide composite Where x= 10, 20 and 30 % of Fe_3SO_4	MRG X
Silver carbonate/ Magnetite/ reduced graphene oxide composite Where x= 25, 50 and 75 % of silver carbonate	MRGS X

Photo-catalytic behavior experiment

In this part, the photocatalytic activities of the composites were performed under pretend visible light irradiation of a halogen lamp (500 W). Composites were added to 60 mL of aqueous TZ (50 ppm) solution, stirring for 25 min in dark, until equilibrium is gained. The composite was collected by magnet and 2-ml of the clear solution is examined by UV–Vis spectroscopy.

Results and discussions

Sample characterization

(Fig. 1(a)) shows the Raman spectra of GO, the primary components in the Raman spectra of graphitic carbon-based materials are the G and D peak. The result revealed that there are two characteristics peaks at 1345 cm^{-1} which is corresponding to D band and the other peak at 1592 cm^{-1} which is corresponding to G band. The D peak is for the aromatic rings and is considered as a measure of the imperfection of the structure. However, the G peak result from the bond of the carbon atom in the rings or in the chain. In addition, the overtone of the D peak which is called as 2D peak appears at 2700 cm^{-1} and related to graphene layers [**47**].

(Fig. 1(b)) shows the Raman spectrum of MRG with different ratio of magnetite. The characteristics peak of RG appears in 1358 cm^{-1} and 1591 cm^{-1}[**48**]. In which the ratio of I_D/I_G was 0.98 GO. While, these ratios were 1.52, 1.14 and 1.09 for MRG10, MRG 20 and MRG 30, respectively. These high ratios in the composite relative to GO revealed that the presence of imperfection in the functionalization of graphene by magnetite and confirming the formation of a chemical bonding during the preparation [**49**]. As is shown in **(Fig. 1(c))**, two characteristic peaks of RG can be observed, the G-band, where is attributed to the E_{2g} vibrational manner of sp^2 bonded carbon and is recognized at 1591 cm^{-1}, and the D-band at 1365 cm^{-1} is owing to the A_1g manner vibrations of six-membered sp^2 carbon rings. The four characteristic peaks, which located at 940cm^{-1}, 1013cm^{-1}, 1120cm^{-1} and 1175cm^{-1} are distinctive to Ag_2CO_3 Raman peaks [**43**]. After the introduction of RG in the MRGS composites, the intensity of the four characteristic peaks demonstrates a significant decrease, which may be due to the wrapped RG on the surface of MRGS [**43**].

FTIR spectrum shows the good bonding of RGO and magnetite, as shown in (**Fig. 2(a)**). The wide-ranging peak located at about (3400 cm^{-1}) was owed to the extending vibration of O-H. The Peak at 600 cm^{-1} can be well-thought-out as a grouping of Fe–O vibrations, representative of the operative combination of magnetite nanoparticles and reduced graphene sheets [**50**]. The absorption band located at 1553 cm^{-1} is linked to the undernourished vibration of reduced graphene sheets, which demonstrates the establishment of RG [**51**].

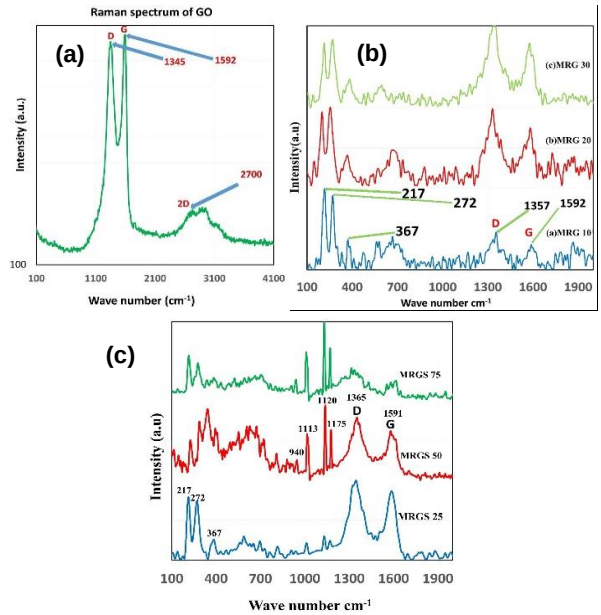

Fig. 1. The Raman spectrum of (a) The prepared sample of graphene oxide GO, (b) The prepared samples of MRG10, MRG 20 and MRG 30, (c) The prepared samples of MRGS 25, MRGS 50 and MRGS 75.

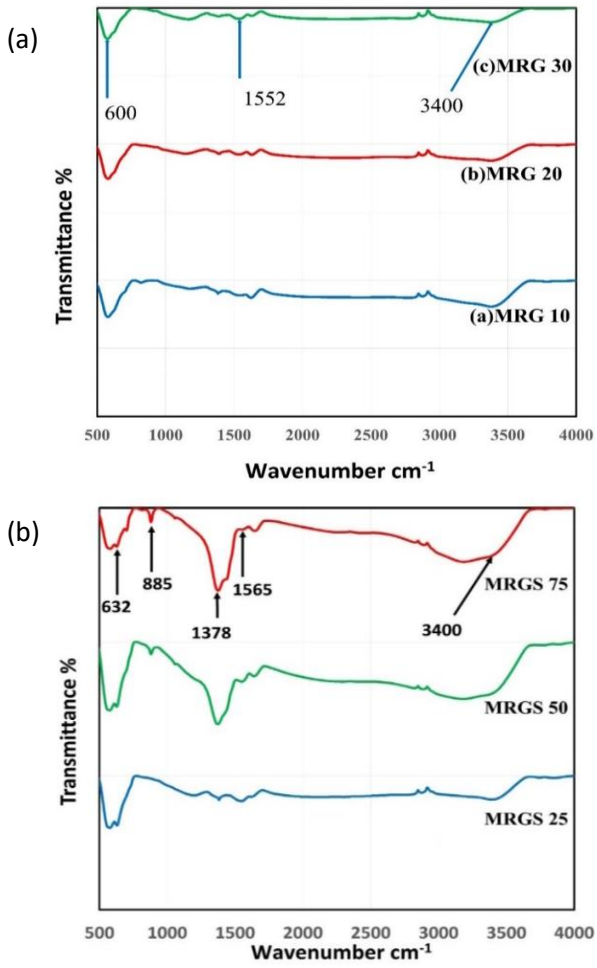

Fig. 2. FTIR spectra of (a) The prepared samples of MRG10, MRG 20 and MRG 30, (b) The prepared samples of MRGS 25, MRGS 50 and MRGS 75.

(**Fig. 2(b)**) gives the FTIR spectra of different composition of the prepared composite. It may be realized that MRGS samples have a peak at 3400 cm^{-1} which is related to the extending vibration and twisting vibration of ⁻OH functional groups on the composite. Peaks at 1565 cm^{-1}, 1378 cm^{-1}, 885 cm^{-1}, and 632 cm^{-1} are linked to the characteristic peaks for CO_3^{-2} [**52, 53**].

(Fig. 3(a)) displays the diffraction peaks at 2Θ of 30.26, 35.70, 43.4, 53.70, 57.4, and 63.2 where they are distinguishing to a lattice plane of cubic magnetite and corresponding to [(220), (311), (400), (422), (511) and (440)] respectively. The spectrum does not show the characteristics peaks of RGO where this may be attributed to the following reasons. Firstly, we assume that the existence of magnetite leads to decreases the accumulation of graphene sheets. Secondly, the sturdy peak of magnetite has the propensity to control the scrawny peak of graphene [**54**].

(Fig. 3(b)) shows the XRD patterns of MRGS composite samples. From this result, we can conclude that Ag_2CO_3 reveal obvious diffraction peaks at 2θ equal 17.57°, 21.51°, 31.53°, 32.63°, 36.9°, 38.5°, 40.8° and 43.33°, which are corresponding to (020), (110), (-101), (-130), (200), (031), (220) and (131) crystalline planes. These planes are indexed to the monoclinic phase of Ag_2CO_3 (JCPDS No: 26-0339). These diffraction peaks are very sharp, the representative high crystallinity of these composite [**52**]. There is no diffraction peaks related to RG were detected in the XRD pattern of MRGS due to the destruction of the regular stacking of graphene layers by the loading of Ag_2CO_3 nanoparticles and also relatively low diffraction intensity of RG [**43**].

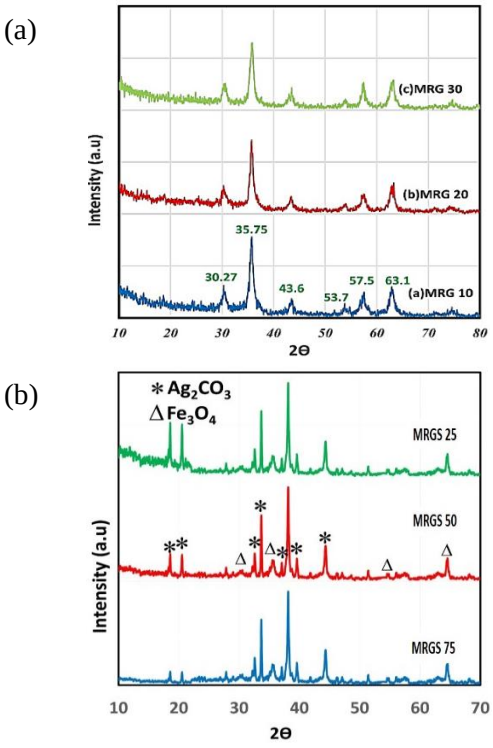

Fig. 3. XRD patterns of (a) The prepared samples of MRGO10, MRGO 20 and MRGO 30, (b) The prepared samples of MRGS 25, MRGS 50 and MRGS 75.

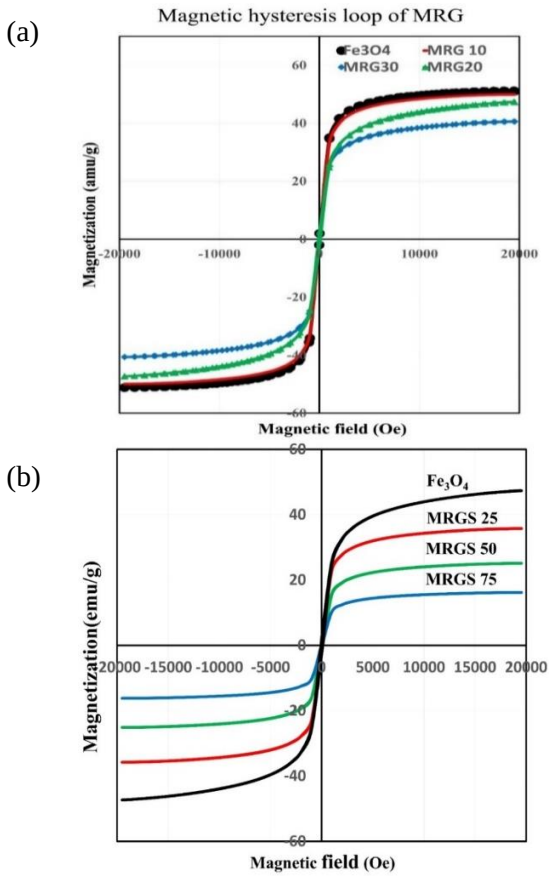

Fig. 4. VSM analysis for of (a) The prepared samples of Fe_3O_4, MRG10, MRG 20 and MRG 30, (b) The prepared samples of MRGS 25, MRGS 50 and MRGS 75.

Vibrating Sample Magnetometer (VSM) of MRG was achieved at ambient temperature and the magnetic performance of MRG 10, 20 and 30 composites are presented in the **(Fig. 4(a))**. The result revealed that magnetization hysteresis loops (S-like curves) were showed for both magnetite nanoparticles and nano-composites, which verified that they have a superparamagnetic performance with a saturation magnetization of 50, 47.3 and 40.6 emu/g for MRG 10, 20 and 30, respectively. It was obvious, that as the graphene content increases in the samples the recorded magnetization values decrease. It could be assumed that the chemical bonding of magnetite on graphene sheets as mentioned previously in the Raman result, may effects negatively on the saturation magnetization of the samples [**55**]. Fe_3O_4 nano-powder demonstrate ferromagnetic performance with a capacity magnetization of 51 emu/g, which was detected to be more than that of MRG nano-composites. The lower magnetization in MRG nano-composites might be ascribed to the presence of RG nano-sheet in the sample [**55, 56**].

(**Fig. 4(b)**) shows the magnetization curves of the MRGS with different proportion. The magnetization value declines from 35.7, 25.1 to 16.1 emu/g for MRG10, MRG 20 and MRG 30, respectively. However, it was 51 emu/g in the bare Fe_3O_4 sample. This may be attributed to the existence of nonmagnetic materials in the surface of MRGS. However, this is still suitable for

the magnetic separation of the sample. Nevertheless, the reversibility in the hysteresis loop confirms that there is no gathering happens to the nano-composite [**57**].

(Fig. 5 (a), (b) and (c)) shows the morphologies by High-Resolution Transmission Electron Microscope (HRTEM) of the Fe_3O_4 with various amounts of RGO (10%, 20%, and 30%, respectively. As shown, the gray part determines the RG nanoparticles, while the dark part determines the accumulation of Fe_3O_4 nanoparticles. The magnetite can be notable obviously in MRG (10 % and 20% respectively). On the other hand at MRGO 30 %, Graphene has a tendency to shelter whole the nanoparticles and hamper the action of these particles [**58**]. The iron peak magnitude decreased with respect to carbon peak from MRG 10 to MRG 30 due to the increase of RG ratio as shown by EDX in **(Fig. 5 (d), (e) and (f))** respectively.

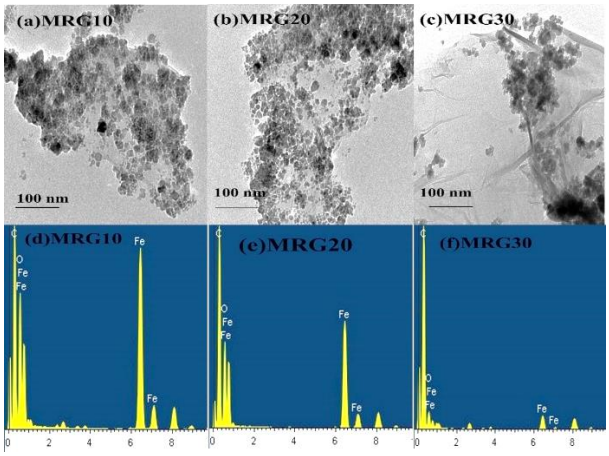

Fig. 5. HRTEM and EDX spectra of (a) and (d) for MRG 10, (b) and (e) for MRG 20, (c) and (f) for MRG 30.

The TEM of the MRGS 25, 50 and 75 composites were observed in **(Fig. 6)**. The MRG sheets were had a good distribution with Ag_2CO_3 nanoparticles, demonstrating loading densities of Ag_2CO_3, which is compatible with the EDX results [**59**].

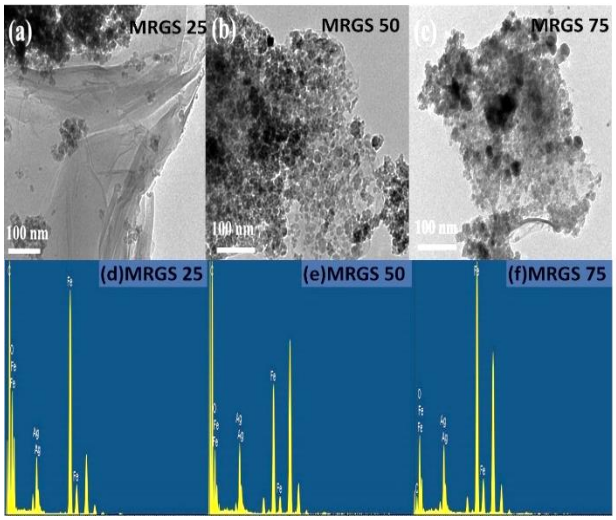

Fig. 6. HRTEM and EDX spectra of (a) and (d) for MRGS 25, (b) and (e) for MRGS 50, (c) and (f) for MRGS 75.

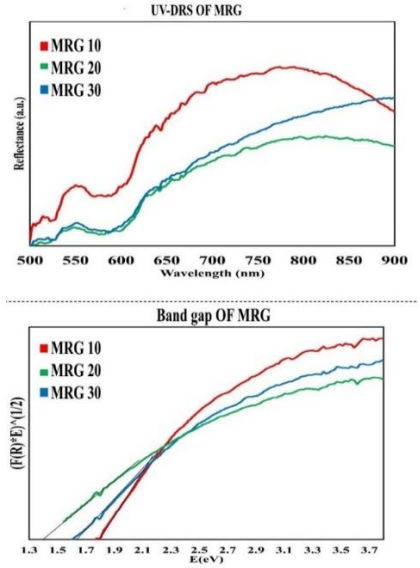

Fig. 7. Diffuse reflectance and the band gap of MRG 10, MRG 20 and MRG 30.

(Fig. 7) Presents UV–vis spectra of MRG 10, 20 and 30 composites. The result of sample MRG 20 has a red alteration for about 25 nm in contrast to MRG 10. This reveals the reduction of the band gap energy. MRG 10, 20 and 30 shows values of band gap energy 1.8, 1.4 and 1.64 eV respectively. The band gap energy values were considered from the $(F(R)h\upsilon)^{1/2}$ against the hυ curve, where F(R)=(1-R)/2R [**60**]. The slight blue change of MRG 30 is attributed to blocking a portion of visible light by rough layers of RG [**61**]. MRG 20 was the superlative ratio which yields the lowest E_g (1.4 ev).x

(Fig. 8) shows the UV-Vis spectra of MRGS composites. The band gaps energy (E_g), of the composites MRGS 25, MRGS 50 and MRGS 75 were calculated and give the following values 1.6, 1.55 and 1.5 eV respectively.

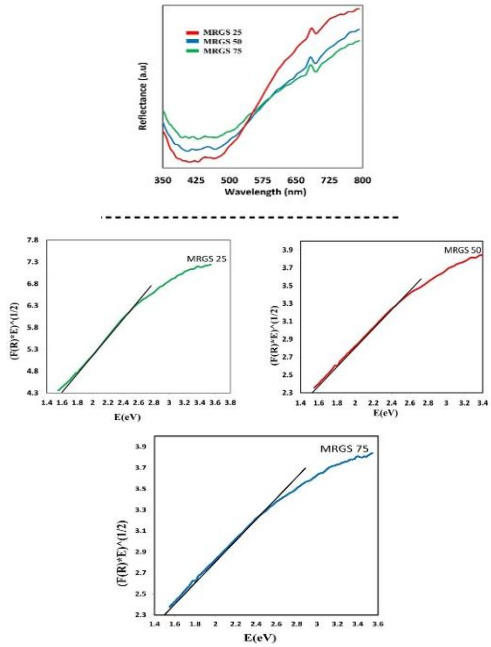

Fig. 8. UV-vis spectra and the band gap energies of MRGS 25, MRGS 50 and MRGS 75.

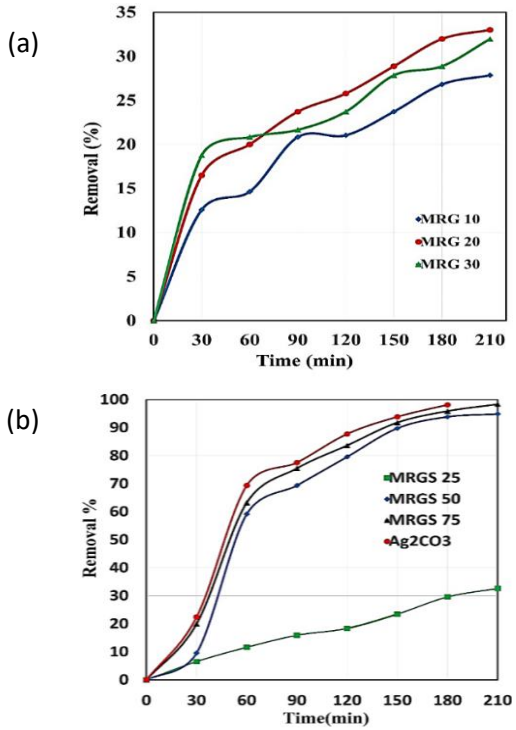

Fig. 9 Photocatalytic degradation of tartrazine by (a) The prepared samples of MRG 10, MRG 20 and MRG 30, (b) The prepared samples of MRGS 25, MRGS 50 and MRGS 75, at room temperature.

The catalytic activity of the prepared composites

In this part, the decomposition of TZ dye in visible light was achieved at ambient temperature. The result showed that the ideal catalyst loading was MRG 20 compared to MRG10 and MRG 30 as shown in **(Fig. 9 (a))**. This may be attributed to, by increasing of the quantity of graphene (RG) on magnetite exterior leads to the whole shelter of nanoparticles and hamper the photo-catalytic effect of these particles [**61**]. This thought harmonized with the results obtained from UV-Vis reflectance and TEM observation.

The decomposition of TZ dye was studied using MRGS 25, 50 and 75 composites, at ambient temperature for 210 min. of illumination. The results of degradation versus time show that the best catalyst was MRGS 75 as shown in **(Fig. 9 (b))**. The result showed that a further increase in the amount of MRG in the composite from 25 to 75 % samples MRGS 25 to MRGS 75 respectively, the degradation efficiency increases due to adsorption effects [**62**]. However, a further increase in the amount of MRG more than 75 % leads to decreases the degradation. In addition, the degradation rate of sample MRGS 75 is approximately equal to the degradation rate of Ag_2CO_3.

These results can be ascribed to different transferring rates of the photo-induced carriers and recombination of electron-hole pairs when different amounts of MRG are loaded in the composite. Moreover, further increase of MRG loading more than 75% in the composite prevents Ag_2CO_3 from absorbing visible light, thus causing a rapid decrease in irradiation passing through the reaction media [**63**]. When the amount of MRG increased over the threshold value, the excessive MRG particles tend to form a relatively thick coat and even aggregate on the surface of Ag_2CO_3, thus hindering the migration of excited electrons from the outer MRG layer to the inner Ag_2CO_3 particles. Consequently, the number of radical is decreases and the photo-degradation of the dye pollutant is thus affected. Therefore, the amount of MRG loading should be adequately controlled [**64,65**].

Table 2 shows that removal-degradation efficiency of TZ using MRGS 75 is significantly higher than other samples available in the literature. Besides, MRGS 75 has magnetic properties to facilitate its extraction from solution.

Table 2. Maximum degradation of various photocatalysts for TZ dye.

Photocatalysts	Started concentration (ppm)	Radiation source	Time (min.)	Degradation (%)	Ref.
Ag-silicon nanowires (SiNWs)	5.5	UV	200	< 10%	[**66**]
Au-(SiNWs)	5.5	UV	200	< 10%	[**66**]
Pt-(SiNWs)	5.5	UV	200	11%	[**66**]
H-SiNWs	5.5	UV	200	27.39%	[**66**]
Pd-(SiNWs)	5.5	UV	200	47.45%	[**66**]
Cu-(SiNWs)	5.5	UV	200	67.45%	[**66**]
Cu-(SiNWs) with H_2O_2	5.5	UV	200	95.48%	[**66**]
N-doped TiO_2	—	Visible	90	50%	[**67**]
N-doped TiO_2 with organic phosphors	—	Visible	90	85%	[**67**]
ZnO	40	UV	60	92.9%	[**68**]
MRG 20	50	Visible	210	33%	This work
MRGS 75	50	Visible	210	98.5%	This work

Reusability of MRGS catalyst for photo-degradation of TZ dye

To study the repeatability of the MRGS75 photo-catalyst, recycle experiments of tartrazine decomposition were performed and shown in **(Fig. 10)**. It was found that the degradation ratio of MRGS 75 to the tartrazine dye decrease from cycle one (98.3%) to cycle five (97.4%) in a very small value which indicates that the photo-catalyst (MRGS 75) has high repeatability after many recycle experiments. This decrease in photo-catalytic activity after each cycle was due to slight aggregation of particle and matrices on the surface of the catalyst, and this prevents excitation of photos during the photo-catalytic degradation process.

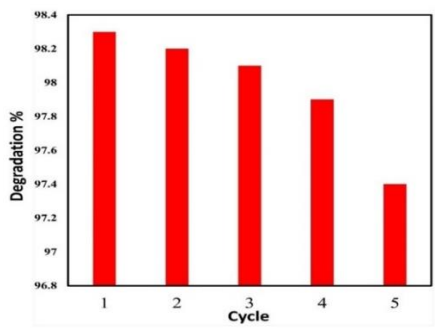

Fig. 10. Stability and reusability of MRGS 75 composite.

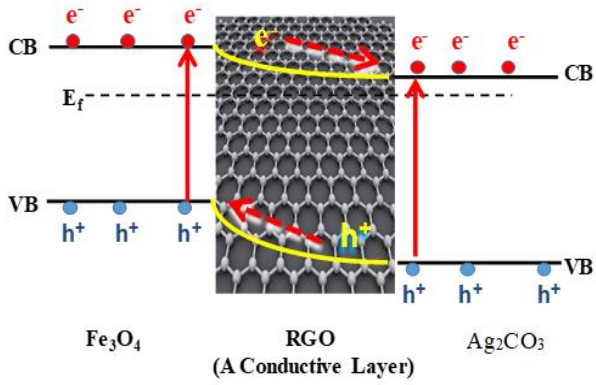

Fig. 11. Mechanism of photo-generated charges in MRGS 75.

Photo-catalytic degradation mechanism

Fig. 11 shows the deprivation mechanism, related to all the obtained results and the energy gap calculations of the structure of Fe_3O_4/RGO/ Ag_2CO_3 (MRGS). Under visible light illumination, Fe_3O_4, RG and Ag_2CO_3 particle absorb photons at their boundary and then electrons and holes are produced in the composite. The produced electrons in the CB of magnetite can move to the CB of Ag_2CO_3 via RG. In this case, RG works as a conductive layer to improve the electron-hole parting [**69-71**].

Where all the techniques, which have been used to characterize the structure of the composite, proved the Janus structure of Fe_3O_4 and Ag_2CO_3 in the presence of the conductive layer (RG). The presence of an interlayer (RG) facilitated the migration of electron into Ag_2CO_3 and accumulated hole in Fe_3O_4. Then $OH^{\bullet}$ radicals have been produced by holes which have strong oxidizing power. In addition, electrons generated photo-chemically can produce $O_2^{\bullet-}$ which play an important role for degradation of tartrazine. The main oxidative species in the Fe_3O_4/RG/ Ag_2CO_3 photo-catalytic process, under visible light irradiations are exogenous radicals ($^{\bullet}O$), hydroxyl radical, ($^{\bullet}OH$) and holes (h^+). That species attack the TZ dye molecule leads to its degradation. The following reactions illustrate the degradation process on the composite surface.

MRGS + hν	→	(h^+) Fe_3O_4 //conductive layer of RG// (e^-) Ag_2CO_3	(1)
(e^-) Ag_2CO_3 + O_2	→	$O_2^{\bullet-}$	(2)
$H_2O + O_2^{\bullet-}$	→	$_2OH^{\bullet}$	(3)
(h^+) Fe_3O_4 + H_2O	→	$OH^{\bullet} + H^+$	(4)
$H_2O + O_2^{\bullet-} + H^+$	→	$OH^{\bullet} + H_2O_2 + OH^-$	(5)
$H_2O_2 + e^-$	→	$OH^{\bullet} + OH^-$	(6)
$OH^- + h^+$	→	$OH^{\bullet}$	(7)
$OH^{\bullet}$ + TZ	→	degradation of tartrazine dye	(8)

Conclusion

In this work, observations specify that RG sheets are completely exfoliated and ornamented with Fe_3O_4 nanoparticles. The photo-catalytic activity experiments show that join Fe_3O_4 and magnetically detachable MRG and MRGS photo-catalyst has been successfully produced. Coupling Ag_2CO_3 nanoparticles with magnetic reduced graphene oxide sheets leads to high photo-catalytic activity in the direction of decomposition of TZ azo-dye under visible light illumination, which reaches more than 95% in short period of time. However, the commercial photo-catalyst TiO_2 is nearly sedentary under visible light. The intended nano-composites were detached easily from the mixture by using an outside magnet after degradation experiment.

References

1. Ahmad, M.; Ahmed, E.; Hong, Z.; Khalid, N.; Ahmed, W.; Elhissi, A.; *J. Alloys Compd*., **2013**, *577*, 717.
2. Huang, X.; Zhou, X.; Wu, S.; Wei, Y.; Qi, X.; Zhang, J.; Boey, F.; Zhang, *H.*; *Small*, **2010**, *6*, 513.
3. Zhang, Y.; Yuan, X.; Wang, Y.; Chen, Y. *J.*; *Mater. Chem*.,**2012**, *22*, 7245.
4. Li, Y.; Gao, W.; Ci, L.; Wang, C.; Ajayan, P. M.; *Carbon*, **2010**, *48*, 1124.
5. Li, Z.; Wu, S.; Ding, H.; Zheng, D.; Hu, J.; Wang, X.; Huo, Q.; Guan, J.; Kan, Q.; *New J. Chem*., **2013**, *37*, 1561.
6. Li, B.; Cao, H. J.; *Mater. Chem*., **2011**, *21*, 3346.
7. Guo, J.; Zhu, S.; Chen, Z.; Li, Y.; Yu, Z.; Liu, Q.; Li, J.; Feng, C.; Zhang, D.; *Ultrason. Sonochem*., **2011**, *18*, 1082.
8. Huang, X.; Zhou, X.; Zhou, L.; Qian, K.; Wang, Y.; Liu, Z.; Yu, C.; *Chem.Phys.Chem*., **2011**, *12*, 278.
9. Wang, G.; Liu, T.; Luo, Y.; Zhao, Y.; Ren, Z.; Bai, J.; Wang, H.; *J. Alloys Compd*., **2011**, *509*, L216.
10. Cheng, Q.; Tang, J.; Ma, J.; Zhang, H.; Shinya, N.; Qin, L.C.; *Carbon*, **2011**, *49*, 2917.
11. Cao, A.; Liu, Z.; Chu, S.; Wu, M.; Ye, Z.; Cai, Z.; Chang, Y.; Wang, S.; Gong, Q.; Liu, Y.; *Advanced materials*, **2010**, *22*, 103.
12. Zhang, Y.; Zhang, N.; Tang, Z.R.; Xu, Y.J. *Acs Nano*, **2012**, *6*, 9777.
13. Li, Y.; Wang, H.; Xie, L.; Liang, Y.; Hong, G.; Dai, H.; *J. Am. Chem. Soc*., **2011**, *133*, 7296.
14. Wang, H.; Cui, L.-F.; Yang, Y.; Sanchez Casalongue, H.; Robinson, J. T.; Liang, Y.; Cui, Y.; Dai, H.; *J. Am. Chem. Soc*., **2010**, *132*, 13978.
15. Yang, N.; Zhai, J.; Wang, D.; Chen, Y.; Jiang, L.; *ACS nano*, **2010**, *4*, 887.
16. Pasricha, R.; Gupta, S.; Srivastava, A. K.; *Small*, **2009**, *5*, 2253.
17. Yoo, E.; Okata, T.; Akita, T.; Kohyama, M.; Nakamura, J.; Honma, *I. Nano Lett*., **2009**, *9*, 2255.
18. Lu, G.; Li, H.; Liusman, C.; Yin, Z.; Wu, S.; Zhang, H.; *Chem. Sci*., **2011**, *2*, 1817.
19. Li, Z.; Yang, B.; Yun, G.; Zhang, S.; Zhang, M.; Zhao, M.; *J. Alloys Compd*., **2013**, *550*, 353.
20. Bin, X.; Chen, J.; Cao, H.; Chen, L.; Yuan, J.; *J. Phys. Chem. Solids*, **2009**, *70*, 1.
21. Wang, Z.; Du, Y.; Zhang, F.; Zheng, Z.; Zhang, Y.; Wang, C. *J.*; *Solid State Electrochem*., **2013**, *17*, 99.
22. Bai, S.; Shen, X.; Zhu, G.; Xu, Z.; Liu, Y.; *Carbon*, **2011,** *49*, 4563.
23. Anandan, S.; Manivel, A.; Ashokkumar, M.; *Fuel Cells*, **2012**, *12*, 956.
24. Xia, X.; Tu, J.; Mai, Y.; Chen, R.; Wang, X.; Gu, C.; Zhao, X.; *Chemistry – A European Journal*, **2011**, *17*, 10898.
25. Wang, P.; Jiang, T.; Zhu, C.; Zhai, Y.; Wang, D.; Dong, S.; *Nano Res*., **2010**, *3*, 794.
26. He, Y.S.; Bai, D.W.; Yang, X.; Chen, J.; Liao, X.-Z.; Ma, Z.F. *Electrochem. Commun*., **2010**, *12*, 570.
27. Wang, H.; Robinson, J. T.; Diankov, G.; Dai, H.; *J. Am. Chem. Soc*., **2010,** *132*, 3270.
28. Wang, H.; Yang, Y.; Liang, Y.; Robinson, J. T.; Li, Y.; Jackson, A.; Cui, Y.; Dai, H.; *Nano Lett*., **2011**, *11*, 2644.
29. Chou, S.L.; Wang, J.Z.; Choucair, M.; Liu, H.K.; Stride, J. A.; Dou, S.X.; *Electrochem. Commun*., **2010**, *12*, 303.
30. Kou, L.; Gao, C.; *Nanoscale*, **2011**, *3*, 519.
31. Yan, J.; Wei, T.; Shao, B.; Ma, F.; Fan, Z.; Zhang, M.; Zheng, C.; Shang, Y.; Qian, W.; Wei, F.; *Carbon*, **2010**, *48*, 1731.
32. Wassei, J. K.; Cha, K. C.; Tung, V. C.; Yang, Y.; Kaner, R. B.; *J. Mater. Chem*., **2011**, *21*, 3391.

33. Lei, Z.; Christov, N.; Zhao, X.; *Energy Environ. Sci*., **2011**, *4*, 1866.
34. Fan, Z.J.; Yan, J.; Wei, T.; Ning, G.Q.; Zhi, L.J.; Liu, J.C.; Cao, D.X.; Wang, G.-L.; Wei, F.; *ACS nano*, **2011**, *5*, 2787.
35. Yu, D.; Park, K.; Durstock, M.; Dai, L.; *The journal of physical chemistry letters*; **2011**, *2*, 1113.
36. Meyer, R. In VII ASPO Conference, Barcelona, Spain, **2008**. http://www. aspo-spain. org/asp07/presentations/Meyer-CSP-ASP07.
37. Lalitha, K.; Reddy, J. K.; Sharma, M. V. P.; Kumari, V. D.; Subrahmanyam, M.; *Int. J. Hydrogen Energy*; **2010**, *35*, 3991.
38. Hu, X.; Hu, C.; *J. Solid State Chem*., **2007**, *180*, 725.
39. Bi, Y.; Hu, H.; Ouyang, S.; Lu, G.; Cao, J.; Ye, J.; *Chemical Communications*, **2012**, *48*, 3748.
40. Park, S.; Lee, J. M.; Jo, Y. K.; Kim, I. Y.; Hwang, S.J.; *Dalton Trans*., **2014**, *43*, 10566.
41. Dong, C.; Wu, K.L.; Wei, X.W.; Wang, J.; Liu, L.; Jiang, B.B. *Appl. Catal. A.*, **2014**, *488*, 11.
42. Dai, G.; Liu, S.; Liang, Y.; Liu, K.; *RSC Adv*., **2014**, *4*, 34226.
43. Dai, G.; Yu, J.; Liu, G.; *The Journal of Physical Chemistry C*, **2012**, *116*, 15519.
44. Tian, N.; Huang, H.; He, Y.; Guo, Y.; Zhang, Y. *Colloids Surf., A* **2015**, *467*, 188.
45. Wang, J.; Shen, J.; Fan, D.; Cui, Z.; Lü, X.; Xie, J.; Chen, M. *Mater. Lett*., **2015**, *147*, 8.
46. Shahriary, L.; Athawale, A. A.; *Int J Renew Energy Environ Eng*, **2014**, *2*, 58.
47. Cheng, J.; Shou, Q.; Wu, J.; Liu, F.; Dravid, V. P.; Zhang, X. *J. Electroanal. Chem*., **2013**, *698*, 1.
48. Min, Y.; Zhang, K.; Zhao, W.; Zheng, F.; Chen, Y.; Zhang, Y.; *Chem. Eng. J*., **2012**, *193*, 203.
49. Gao, Y.; Zhong, D.; Zhang, D.; Pu, X.; Shao, X.; Su, C.; Yao, X.; Li, S.; *J. Chem. Technol. Biotechnol*., **2014**, *89*, 1859.
50. Sher Shah, M. S. A.; Park, A. R.; Zhang, K.; Park, J. H.; Yoo, P.; *J. ACS Appl. Mater. Interfaces*, **2012**, *4*, 3893.
51. Li, J.; Wei, L.; Yu, C.; Fang, W.; Xie, Y.; Zhou, W.; Zhu, L.; *Appl. Surf. Sci*., **2015**, *358*, 168.
52. Song, Y.; Zhu, J.; Xu, H.; Wang, C.; Xu, Y.; Ji, H.; Wang, K.; Zhang, Q.; Li, H.; *J. Alloys Compd*., **2014**, *592*, 258.
53. Yang, X.; Chen, C.; Li, J.; Zhao, G.; Ren, X.; Wang, X.; *RSC Adv*., **2012,** *2*, 8821.
54. Boruah, P. K.; Borah, D. J.; Handique, J.; Sharma, P.; Sengupta, P.; Das, M. R., *J. Environ. Chem. Eng*., **2015,** *3*, 1974.
55. Deng, F.; Lu, X.; Pei, X.; Luo, X.; Luo, S.; Dionysiou, D. D.; *J. Hazard. Mater*., **2017**.
56. Tabrizian, E.; Amoozadeh, A.; *Catal. Sci. Technol*., **2016**, *6*, 6267.
57. El-Maghrabi, H. H.; Nada, E. A.; Soliman, F. S.; Moustafa, Y. M.; Amin, A. E.S., *Egypt. J. Pet*., **2016**.
58. Shi, M.; Shen, J.; Ma, H.; Li, Z.; Lu, X.; Li, N.; Ye, M.; *Colloids Surf., A.*, **2012**, *405*, 30.
59. Lindberg, J. D.; Snyder, D. G.; *Appl. Opt*., **1973**, *12*, 573.
60. El-Maghrabi, H. H.; Abdelmaged, S. M.; Nada, A. A.; Zahran, F.; El-Wahab, S. A.; Yahea, D.; Hussein, G.; Atrees, M.; *J. Hazard. Mater.*, **2017**, *322*, 370.
61. Elsayed, M.; Gobara, M.; *Mater. Res. Express*, **2016**, *3*, 085301.
62. Nada, A. A.; Tantawy, H. R.; Elsayed, M. A.; Bechelany, M.; Elmowafy, M. E.; *Solid State Sci*., **2018,** *78*, 116.
63. Ao, Y.; Wang, P.; Wang, C.; Hou, J.; Qian, *J., Appl. Surf. Sci*. **2013**, *271*, 265.
64. Elsayed, M.; Gobara, M.; Elbasuney, S. J., *Photochem. Photobiol., A* **2017**, *344*, 121.
65. Naama, S.; Hadjersi, T.; Menari, H.; Nezzal, G.; Ahmed, L. B.; Lamrani, S.; *Mater. Res. Bull*., **2016**, *76*, 317.
66. Vaiano, V.; Sacco, O.; Iervolino, G.; Sannino, D.; Ciambelli, P.; Liguori, R.; Bezzeccheri, E.; Rubino, A. *Appl. Catal., B*, **2015**, *176*, 594.
67. Behnajady, M.; Modirshahla, N.; Hamzavi, R., *J. Hazard. Mater*., **2006**, *133*, 226.
68. Hou, Y.; Zuo, F.; Dagg, A.; Feng, P., *Nano Lett*., **2012**, *12*, 6464.
69. Wu, W.; Jiang, C.; Roy, V. A.; *Nanoscale*, **2015**, *7*, 38.
70. Nada, A. A.; Nasr, M.; Viter, R.; Miele, P.; Roualdes, S.; Bechelany, M.; *The Journal of Physical Chemistry C*, **2017**, *121*, 24669.

